Spin imaging of Poiseuille flow of a viscous electronic fluid

K. S. Denisov [ORCID],[*] K. A. Baryshnikov [ORCID], and P. S. Alekseev [ORCID]
Ioffe Institute, 194021 St. Petersburg, Russia

Recent progress in fabricating high-quality conductors with small densities of defects has initiated studies of a viscous electron fluid and has motivated the search for evidence of a hydrodynamic regime of electron transport. In this Letter we come up with the spin imaging technique, which can allow to attest to the emergence of electron hydrodynamic flows. Using numerical calculations, we examine specific inhomogeneous distributions of the electron spin density injected in a sample with a Poiseuille flow of a viscous electron fluid. We also demonstrate that the Hanle curves (the dependencies of the electron spin on magnetic field) at different positions across the channel acquire relative phase shifts resulting from the space variation of the hydrodynamic velocity. The studied effects can be employed to detect and map a viscous electron fluid noninvasively.

In high-quality conductors with small densities of defects, electrons can form a viscous fluid at low temperatures due to frequent electron-electron collisions. The charge transport in such a fluid is carried out by inhomogeneous hydrodynamic flows, controlled by the particular shapes of the samples, while its resistance becomes proportional to the viscosity coefficient. These ideas were first proposed and theoretically developed for bulk metals with strong electron-phonon coupling [1]. Recently, this topic has become of interest as a hydrodynamic regime of electron transport has been realized in high-quality samples of graphene [2–8], high-mobility GaAs quantum wells [9–22], quasi-two-dimensional metal PdCoO$_2$ [23], and the Weyl semimetal WP$_2$ [24]. These experiments motivated many theoretical works (see, for example, Refs. [25–41]), which were aimed to formulate and search for evidence of the hydrodynamic regime as well as to study various types of flows.

Evidence of the formation of a viscous electron fluid is based, first, on an inhomogeneity of space distributions of its flows, leading to specific properties of the observed sample resistances. The simplest of these properties is the cubic dependence of conductance on the sample width. This dependence was observed for the first time in Ref. [23] for stripes of PdCoO$_2$. In samples with a peculiar geometry of edges and contacts, whirlpools can appear, similarly to water flows in rivers. Thus the opposite directions of the current and a voltage drop appear for some pairs of contacts. This effect of "absolute negative resistance" was proposed as evidence of viscous flows of electrons in Ref. [6] and was observed for graphene samples in Ref. [2]. Second, the dependencies of electron viscosity on magnetic field and flow frequency are very specific and can be used to characterize a viscous electron fluid. The giant negative magnetoresistance observed on high-mobility GaAs quantum wells [12–15] was explained by this effect and thereby was employed to detect hydrodynamic

transport [16]. For ac flows of an electron fluid, the viscosity exhibits resonance at a doubled electron cyclotron frequency [38,39]. Such resonance manifests itself in responses of the fluid conductance on incident radiation, that was apparently observed in Refs. [9,20,21]. In particular, in a strongly non-ideal electron fluid the ac flow is formed by transverse shear stress waves, whose dispersion law reflects the resonance in the viscosity coefficients. In recent works [7,8] direct observations of the profiles of the Hall electric field and the current density for a Poiseuille flow of two-dimensional (2D) electrons in graphene stripes by means of space-resolved measurements of electric and magnetic fields were reported.

All these methods are quite difficult to use: They require either an analysis of data on a number of specially designed samples with a given geometry or applying sufficiently strong magnetic fields. Therefore, simpler, weaker-invasive methods are desired.

In this Letter we propose a spin-injection-based method to detect and map the hydrodynamic regime of electric transport (see Fig. 1). Namely, we demonstrate that the space distribution of the injected spins can be employed to visualize a viscous flow of an electron fluid ("spin imaging technique"). In particular, the distributions of the electron spin density and its magnetic field dependence for the Poiseuille flow of a viscous electron fluid strongly differs from the Ohmic regime. We demonstrate this concept by performing numerical calculations with realistic parameters for GaAs quantum well high-mobility samples.

The advantage of the proposed method is that the injected spin distribution has almost no effect on a given electron flow. In this way, the proposed technique is "light and noninvasive," as compared with the already existing methods of detection of the viscous electron fluid. In addition, measuring spin distributions with high accuracy and resolution is a well-developed technique [42,43].

We consider a flow of 2D viscous electron fluid in high-mobility samples, where the length of the electron scattering on impurities l_{tr} can be longer than the one of the electron-
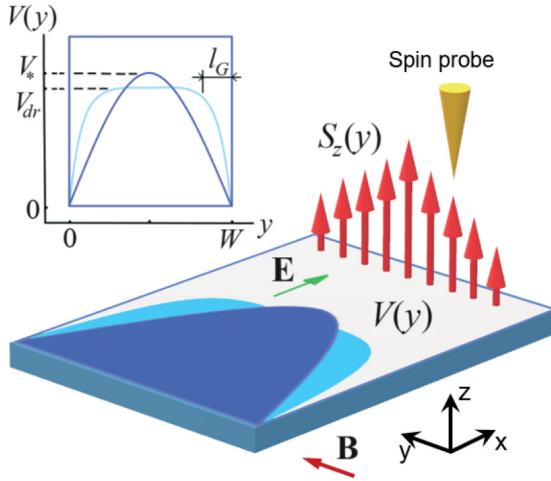
___

[*]denisokonstantin@gmail.com

FIG. 1. Scheme of the proposed spin imaging technique. Light and dark blue curves depict the electron flow velocity $V(y)$ under electric field $\boldsymbol{E}$ for the Poiseuille and Ohmic-like regimes, respectively. Spin-polarized electrons are injected from the contact located at $x = 0$. The spin polarization $S_z(y)$ (indicated by red arrows) exhibits an inhomogeneous profile reflecting the profile $V(y)$ and can be detected by a local spin probe. Inset: Profiles of the Poiseuille and the Ohmic-like flows.

electron collisions l_{ee}. In this regime the electron momentum relaxation takes place predominantly or mostly at the channel boundaries with the subsequent formation of the Poiseuille flow.

In the case of long and sufficiently wide samples, $W \gg l_{ee}$ (realized, for example, in experiments [7,8,17–19]), the velocity distribution can be found from the Navier-Stokes equation with an added bulk relaxation term. The result for stationary flows in samples with some density of defects and fully rough edges takes the form [1]

$$V_x(y) = \frac{e\,E_x}{m\,\tau_{tr}} \left\{ 1 - \frac{\cosh[(y - W/2)/l_G]}{\cosh[(W/2)/l_G]} \right\}, \qquad (1)$$

where m is an electron mass; W is the channel width; τ_{tr} is the momentum relaxation time in the bulk due to scattering of electrons on disorder or phonons; $l_G = \sqrt{\eta \tau_{tr}}$ is the Gurzhi length yielding the width of the near-edge layer in Ohmic flow where the viscosity effect is substantial; $\eta = v_F^2 \tau_{ee}/4$ is the viscosity of the electron fluid determined by electron-electron collisions; $\tau_{ee} = l_{ee}/v_F$ is the time of relaxation of the shear stress due to interparticle collisions; and v_F is the Fermi velocity. Equation (1) describes the homogeneous Ohmic flow $V_{dr} = e\,E_x/(m\,\tau_{tr})$ at $l_G \ll W$, while the Poiseuille parabolic distribution appears in the opposite limit $l_G \gtrsim W$ [see Fig. 1, where we also use the notation $V_* = V(W/2)$]. Note that although inhomogeneous distributions of the spin density will be studied below, the particle density n is assumed to be homogeneous. Perturbations of n appear for nonstationary flows, formed by plasmons, or when a perpendicular magnetic field is applied (see, for example, Ref. [39]).

We address systems with no pronounced effects of spin-orbit coupling on electric current distribution and neglect the near-boundary spin accumulation due to the spin Hall

effect [44–46] or the rotational viscosity effect [47–51]. In the latter, a vorticity of the electron flow induces a torque acting on the electron spin and results in the generation of the spin density [47]. In other words, our consideration is valid for systems where the electric current profile is settled according to Eq. (1), while the distribution of the spin density follows the local drift velocity of the electron fluid and does not affect its orbital motion. In this approximation the distribution of the spin density $\boldsymbol{S}$ is determined from the drift-diffusion model [52] given by the following equations,

$$\dot{\boldsymbol{S}} + \nabla_i \boldsymbol{q}^i = [\boldsymbol{\Omega}_L \times \boldsymbol{S}] - \boldsymbol{S}/\tau_s, \qquad (2)$$

where ∇_i denotes the partial derivative $\partial/\partial x_i$, $\boldsymbol{q}^i$ is the spin current (the flow of the value $\boldsymbol{S}$ along the direction x_i), $\boldsymbol{\Omega}_L$ is the Larmor precession frequency due to the in-plane magnetic field, and τ_s is the spin relaxation time, which is assumed to be isotropic. The spin current $\boldsymbol{q}^i$ in Eq. (2) contains two contributions,

$$\boldsymbol{q}^i = -D_s \nabla_i \boldsymbol{S} + V_i \boldsymbol{S}, \qquad (3)$$

where the first term describes the spin diffusion with coefficient D_s and the second term stems from the drag of the spin density with the drift velocity $\boldsymbol{V} = \boldsymbol{e}_x V_x(y)$ determined by Eq. (1). In Eq. (3) we omit the shear-viscosity-like term $\sim \Delta_L \boldsymbol{q}^i$ since for conventional electron fluids it is small to the extent of the parameter $l_{ee}^2/a_{char}^2 \ll 1$ (see, for example, Ref. [46]; here, Δ_L is the Laplace operator and a_{char} is the characteristic length scale of flow inhomogeneity).

For further consideration we also use the spin diffusion length $L_s = \sqrt{D_s \tau_s}$ and the spin drift length $L_d = V_* \tau_s$ in the center of the channel, $V_* = V_x(W/2)$.

In general, the spin diffusion length in high-mobility samples can be extremely large due to long momentum relaxation times τ_{tr}. For instance, in clean graphene-based lateral spin valves the spin can diffuse to a distance of up to 1 μm [53–55]. However, when the viscous electron fluid is formed, $D_s = v_F^2 \tau'_{ee}/2$ is significantly reduced [43] as it is mostly governed by electron-electron scattering, where τ'_{ee} describes the relaxation of spin current density [46]. By this means the spin relaxation time τ_s is controlled by the Dyakonov-Pelel-like mechanism giving $1/\tau_s \sim \Omega_{so}^2 \tau'_{ee}$ [56,57]. The decrease of L_s due to the interparticle scattering is favorable for the spin imaging of the Poiseuille flow, as the weakening of the spin diffusion prevents distortion of an inhomogeneous spin pattern.

In order to calculate the distribution of the spin flow and the spin density, we used the boundary conditions of the absence of spin current: $q_y^z = 0$ at the edges $y = 0$ and $y = W$. We assumed that at the contact at $x = 0$ the spin current q_x^z is proportional to the electric current and the fixed spin polarization of electrons in the ferromagnetic contact [52]. In the considered geometry, we take $q_x^z = C V_x(y)$, where C is a constant. This condition is consistent with the hydrodynamic distribution (1) of the electric current. We recognize that the electric current distribution right in the vicinity of a contact ($x \lesssim W$) can change from the Poiseuille form. However, beyond this transition region the hydrodynamic velocity will be settled according to Eq. (1). It is essential that the spin polarization density $S_z(x, y)$ is strongly inhomogeneous.
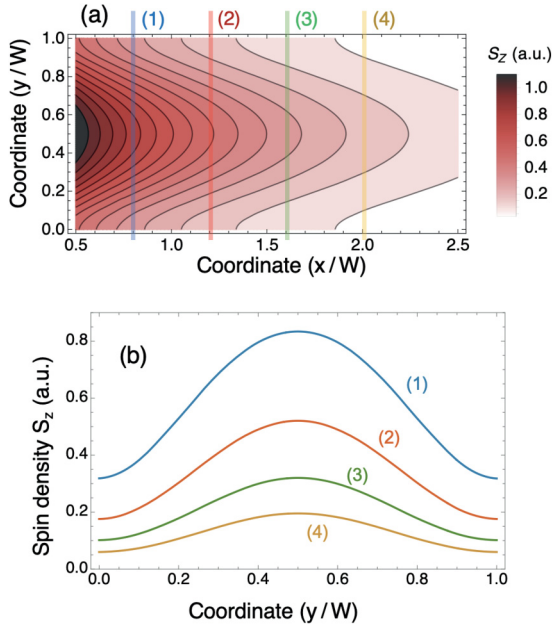
FIG. 2. (a) Calculated distribution of spin polarization in a viscous electron fluid over the channel. (b) Profiles of spin density at different x positions: $x = 0.6W$ (1), $x = 1.2W$ (2), $x = 1.6W$ (3), and $x = 2W$ (4). In the calculations we used parameters typical for high-mobility GaAs quantum well samples: $\tau_s = 200$ ps, $D_s = 60$ cm^2/s ($L_s \approx 1.1$ μm), $V_* = 4 \times 10^6$ cm/s ($L_d = 8$ μm), and $W = 8$ μm.

The calculated distribution of spin density S_z emerging in the Poiseuille flow of electrons is shown in Fig. 2. The parameters are relevant for high-mobility GaAs quantum wells [43,57] and are described in the caption to Fig. 2. Note that the profile along the cross-section coordinate y becomes more inhomogeneous at larger distances x from the contact. This feature is due to a more effective dragging in the center of the channel than near the edges. From Refs. [42,43], one can see that, for example, the Kerr-rotation microspectroscopy allows us to resolve spin distributions at least on a 0.5-μm scale, which is sufficient to observe the spin distributions presented in Fig. 2.

The tail (at large x) of the spin distribution $S_z(x, y)$ presented in Fig. 2(b) can be approximated by simple analytical expressions. For the slowest decaying solution by x we obtained

$$S_z(x, y) = A \, e^{-x/L_*}\left[1 - \Delta_c \cos\left(\frac{2\pi y}{W}\right)\right], \quad (4)$$

where A is a constant being independent of x and y, the factor e^{-x/L_*} describes the spin density decay with an averaged drift length $L_* = \langle V_x\tau_s\rangle = 2L_d/3$, and the parameter Δ_c determines the contrast of the spin distribution. Note that approximate formula (4) neglects the dependence of the shape of the profile of $S_z(y)$ on the coordinate x. It follows from Eq. (4) that imaging of the Poiseuille flow by spin injection is well distinguishable provided that $\Delta_c \sim 1$.

In order to determine the critical set of parameters beyond which Δ_c becomes too small we derive an approximated analytical solution for Eq. (2). We use the biharmonic approx-
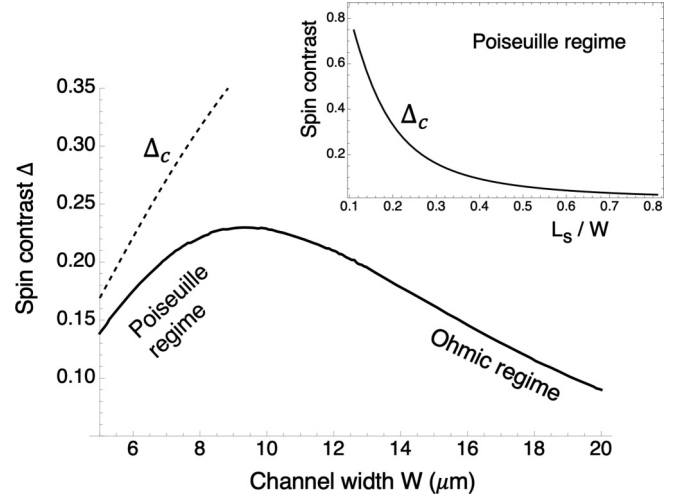

FIG. 3. Dependence of the spin polarization contrast Δ across the channel on its width W. The parameter Δ_c from Eq. (4), which provides the approximate value of Δ in the Poiseuille regime, is shown by the dashed curve. Inset: Dependence of the contrast parameter Δ_c on the ratio L_s/W, characterizing the strength of the spin diffusion, for the Poiseuille regime.

imation for the y dependence of $S_z(x, y)$ and $V_x(y)$ and take into account only the drift component of q_x^z. We obtain $\Delta_c = 6/[2\pi^4\xi^2 + \sqrt{18 + 72\pi^2\xi^2 + 4\pi^8\xi^4}]$, where $\xi = L_s/W$. Expression (4) with such Δ_c is valid in the range $1 \gtrsim \xi \gtrsim 0.05$, where the right boundary is determined by the failure of the biharmonic approximation due to a weakened spin diffusion. The spin distribution plotted in Fig. 2 has the parameters $\xi = 0.14$, $\Delta_c = 0.52$, and the expression from Eq. (4) fits well with the numerical solution starting from $x/W \gtrsim 1.2$.

The dependence of Δ_c on the ratio L_s/W is shown in the inset of Fig. 3. It is seen that the spin contrast decreases significantly, $\Delta_c \lesssim 0.2$, already at moderately strong spin diffusion, $\xi \gtrsim 0.3$, instead of $\xi \gtrsim 1$, as it might be expected. Since Δ_c is determined by the single ratio L_s/W, the applicability of the spin imaging approach for sufficiently large in-plane electric fields (when $L_d \gg L_s$) is governed by simple criteria $W \gtrsim 3L_s$, suggesting that a more plausible situation is realized for sufficiently wide samples.

The spin contrast across the transition between the Poiseuille and the Ohmic transport regimes is illustrated in the main panel of Fig. 3, where we present the dependence of $\Delta = [S_z(y_c) - S_z(y_e)]/[S_z(y_c) + S_z(y_e)]$ on the sample width W calculated at $x = 12$ μm. Here, $y_c = W/2$ is the center of the channel and $y_e = W/10$ is a point near its edge. A nonmonotonic dependence $\Delta(W)$ stems, first, from the fast increase of $\Delta_c(L_s/W)$ due to the suppression of the role of the spin diffusion in a Poiseuille flow with the increase of W, and, second, from the transition to the Ohmic regime where the distributions $V(y)$ and $S_z(y)$ become homogeneous except for the near-edge layers (see Fig. 1).

Next, we study the effect of an in-plane magnetic field $\mathbf{B}\|\mathbf{e}_y$ on the distribution of the injected spin density. Note that in the drift-dominated regime the difference between two Larmor frequencies $\Delta\Omega_L$ at which the Hanle curve (the dependence of $S_{z,x}$ on $\Omega_L\tau_s$) exhibits the neighboring peaks
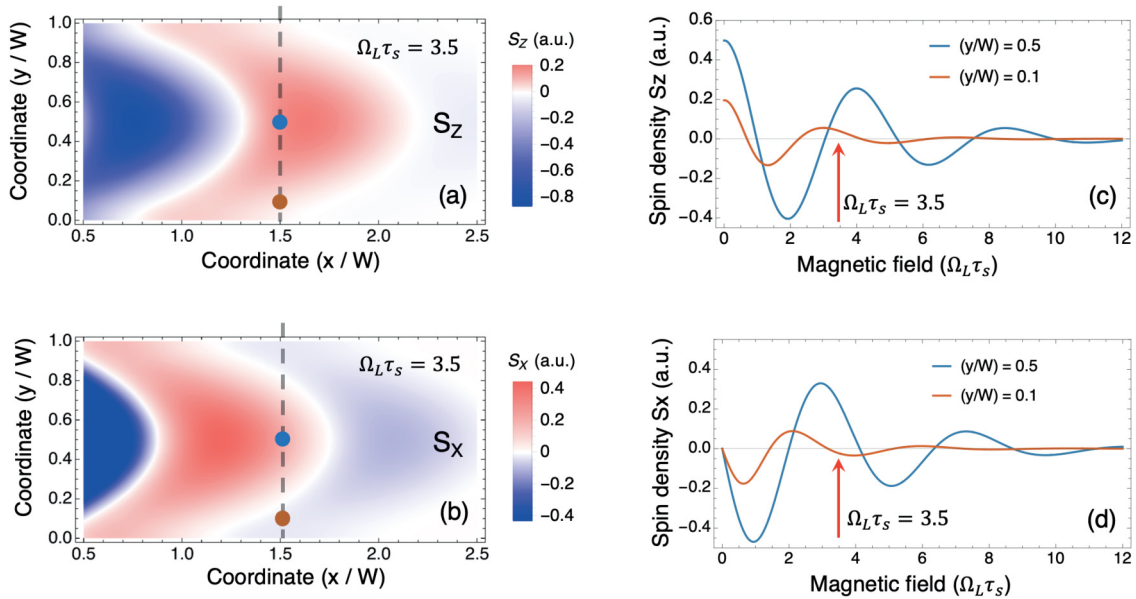
FIG. 4. Distribution of the spin density in a magnetic field directed along the y axis. (a), (b) Space-resolved densities S_z and S_x at $\Omega_L \tau_s = 3.5$. (c), (d) Magnetic field dependencies of S_z and S_x calculated at $x_0 = 12\ \mu$m away from the injector. The Hanle curves on the right panels are taken at the center ($y = 0.5W$, blue color) and near the edge ($y = 0.1W$, orange color) of the channel. The positions of spin detection in each case are depicted by big dots of corresponding colors on the left panels. The parameters of the sample are the same as in Fig. 2.

or dips at a fixed point in space can be estimated as $\Delta\Omega_L = (2\pi V_x)/x_0$, where x_0 is the distance from the injector. In the case of Poiseuille flow, the drift velocity $V_x(y)$ from Eq. (1) changes significantly across the channel. A manifestation of this feature is the shift $\Delta\Omega_L$ as a function of the y coordinate at fixed distance x_0. This effect can be called the "desynchronization" of the Hanle curves and it can serve as more evidence of the formation of a viscous electron flow.

We proceed by considering this effect in more detail. We keep only the injection of the S_z spin component. In Figs. 4(a) and 4(b) we plotted the inhomogeneous spatial patterns of S_z, S_x calculated by Eqs. (1)–(3) with the same boundary conditions at fixed magnetic field $\Omega_L\tau_s = 3.5$ (red and blue colors stand for the positive and negative signs, respectively). The distribution of the spin density visible in Fig. 4 is specific for the drift-dominated regime of the spin transport [52]. Importantly, $S_{z,x}$ are sign altering and inhomogeneous at the same time. One can see that at a fixed distance x_0 the spin density can have different signs in the center and near the boundary of the channel. This feature is explicitly connected with the strong inhomogeneity of the hydrodynamic velocity.

The relative shifts of the oscillation periods $\Delta\Omega_L$ of the Hanle curves are seen in Figs. 4(c) and 4(d). The Hanle curves are calculated at the two spatial positions across the channel [see Figs. 4(a) and 4(b)]. When $\Omega_L\tau_s \sim 4$, these shifts are up to π. We argue that the presented desynchronization of the Hanle curves upon a hydrodynamical response can be used to confirm independently the formation of the viscous electron fluid.

In conclusion, we have proposed an approach to visualize hydrodynamic flows of an electron fluid by measuring the spin polarization distribution across the transport channel. Based on our calculations, we show that measuring both the spin polarization contrast and the Hanle curves at the center and near the boundary of the channel allows one to detect the hydrodynamic regime. We believe that the proposed method paves the way towards noninvasive studies of hydrodynamic viscous electron fluids in samples of different geometry and microscopic structure.

[1] R. N. Gurzhi, Sov. Phys. Usp. **11**, 255 (1968).

[2] D. A. Bandurin, I. Torre, R. K. Kumar, M. Ben Shalom, A. Tomadin, A. Principi, G. H. Auton, E. Khestanova, K. S. Novoselov, I. V. Grigorieva et al., Science **351**, 1055 (2016).

[3] R. Krishna Kumar, D. A. Bandurin, F. M. D. Pellegrino, Y. Cao, A. Principi, H. Guo, G. H. Auton, M. Ben Shalom, L. A. Ponomarenko, G. Falkovich et al., Nat. Phys. **13**, 1182 (2017).

[4] A. I. Berdyugin, S. G. Xu, F. M. D. Pellegrino, R. Krishna Kumar, A. Principi, I. Torre, M. Ben Shalom, T. Taniguchi, K. Watanabe, I. V. Grigorieva et al., Science **364**, 162 (2019).

[5] S. Samaddar, J. Strasdas, K. Janßen, S. Just, T. Johnsen, Z. Wang, B. Uzlu, S. Li, D. Neumaier, M. Liebmann et al., Nano Lett. **21**, 9365 (2021).

[6] L. Levitov and G. Falkovich, Nat. Phys. **12**, 672 (2016).

[7] J. A. Sulpizio, L. Ella, A. Rozen, J. Birkbeck, D. J. Perello, D. Dutta, M. Ben-Shalom, T. Taniguchi, K. Watanabe, T. Holder et al., Nature (London) **576**, 75 (2019).

[8] M. J. H. Ku, T. X. Zhou, Q. Li, Y. J. Shin, J. K. Shi, C. Burch, L. E. Anderson, A. T. Pierce, Y. Xie, A. Hamo et al., Nature (London) **583**, 537 (2020).

[9] Y. L. Dai, R. R. Du, L. N. Pfeiffer, and K. W. West, Phys. Rev. Lett. **105**, 246802 (2010).

[10] A. C. Keser, D. Q. Wang, O. Klochan, D. Y. H. Ho, O. A. Tkachenko, V. A. Tkachenko, D. Culcer, S. Adam, I. Farrer, D. A. Ritchie *et al.*, Phys. Rev. X **11**, 031030 (2021).

[11] A. Gupta, J. J. Heremans, G. Kataria, M. Chandra, S. Fallahi, G. C. Gardner, and M. J. Manfra, Phys. Rev. Lett. **126**, 076803 (2021).

[12] A. T. Hatke, M. A. Zudov, J. L. Reno, L. N. Pfeiffer, and K. W. West, Phys. Rev. B **85**, 081304(R) (2012).

[13] R. G. Mani, A. Kriisa, and W. Wegscheider, Sci. Rep. **3**, 2747 (2013).

[14] L. Bockhorn, P. Barthold, D. Schuh, W. Wegscheider, and R. J. Haug, Phys. Rev. B **83**, 113301 (2011).

[15] Q. Shi, P. D. Martin, Q. A. Ebner, M. A. Zudov, L. N. Pfeiffer, and K. W. West, Phys. Rev. B **89**, 201301(R) (2014).

[16] P. S. Alekseev, Phys. Rev. Lett. **117**, 166601 (2016).

[17] G. M. Gusev, A. D. Levin, E. V. Levinson, and A. K. Bakarov, AIP Adv. **8**, 025318 (2018).

[18] A. D. Levin, G. M. Gusev, E. V. Levinson, Z. D. Kvon, and A. K. Bakarov, Phys. Rev. B **97**, 245308 (2018).

[19] G. M. Gusev, A. D. Levin, E. V. Levinson, and A. K. Bakarov, Phys. Rev. B **98**, 161303(R) (2018).

[20] A. T. Hatke, M. A. Zudov, L. N. Pfeiffer, and K. W. West, Phys. Rev. B **83**, 121301(R) (2011).

[21] M. Bialek, J. Lusakowski, M. Czapkiewicz, J. Wrobel, and V. Umansky, Phys. Rev. B **91**, 045437 (2015).

[22] X. Wang, P. Jia, R.-R. Du, L. Pfeiffer, K. Baldwin, and K. West, arXiv:2205.10196.

[23] P. J. W. Moll, P. Kushwaha, N. Nandi, B. Schmidt, and A. P. Mackenzie, Science **351**, 1061 (2016).

[24] J. Gooth, F. Menges, N. Kumar, V. Süß, C. Shekhar, Y. Sun, U. Drechsler, R. Zierold, C. Felser, and B. Gotsmann, Nat. Commun. **9**, 4093 (2018).

[25] T. Scaffidi, N. Nandi, B. Schmidt, A. P. Mackenzie, and J. E. Moore, Phys. Rev. Lett. **118**, 226601 (2017).

[26] H. Guo, E. Ilseven, G. Falkovich, and L. S. Levitov, Proc. Natl. Acad. Sci. USA **114**, 3068 (2017).

[27] A. Lucas, Phys. Rev. B **95**, 115425 (2017).

[28] F. M. D. Pellegrino, I. Torre, and M. Polini, Phys. Rev. B **96**, 195401 (2017).

[29] P. S. Alekseev, I. V. Gornyi, A. P. Dmitriev, V. Y. Kachorovskii, and M. A. Semina, Semiconductors **51**, 766 (2017).

[30] A. Lucas and K. C. Fong, J. Phys.: Condens. Matter **30**, 053001 (2018).

[31] O. Kashuba, B. Trauzettel, and L. W. Molenkamp, Phys. Rev. B **97**, 205129 (2018).

[32] R. Moessner, P. Surówka, and P. Witkowski, Phys. Rev. B **97**, 161112(R) (2018).

[33] M. Semenyakin and G. Falkovich, Phys. Rev. B **97**, 085127 (2018).

[34] A. Lucas and S. Das Sarma, Phys. Rev. B **97**, 115449 (2018).

[35] R. Cohen and M. Goldstein, Phys. Rev. B **98**, 235103 (2018).

[36] P. S. Alekseev, Phys. Rev. B **98**, 165440 (2018).

[37] J. Y. Khoo and I. S. Villadiego, Phys. Rev. B **99**, 075434 (2019).

[38] P. S. Alekseev, Semiconductors **53**, 1367 (2019).

[39] P. S. Alekseev and A. P. Alekseeva, Phys. Rev. Lett. **123**, 236801 (2019).

[40] K. Trachenko and V. V. Brazhkin, Sci. Adv. **6**, eaba3747 (2020).

[41] P. S. Alekseev and M. A. Semina, Phys. Rev. B **100**, 125419 (2019).

[42] Y. K. Kato, R. C. Myers, A. C. Gossard, and D. D. Awschalom, Science **306**, 1910 (2004).

[43] S. Anghel, F. Passmann, A. Singh, C. Ruppert, A. V. Poshakinskiy, S. A. Tarasenko, J. N. Moore, G. Yusa, T. Mano, T. Noda *et al.*, Phys. Rev. B **97**, 125410 (2018).

[44] M. I. Dyakonov, Phys. Rev. Lett. **99**, 126601 (2007).

[45] P. S. Alekseev and M. I. Dyakonov, Phys. Rev. B **100**, 081301(R) (2019).

[46] M. M. Glazov, 2D Mater. **9**, 015027 (2022).

[47] M. Matsuo, Y. Ohnuma, and S. Maekawa, Phys. Rev. B **96**, 020401(R) (2017).

[48] M. Matsuo, D. A. Bandurin, Y. Ohnuma, Y. Tsutsumi, and S. Maekawa, arXiv:2005.01493.

[49] R. Takahashi, M. Matsuo, M. Ono, K. Harii, H. Chudo, S. Okayasu, J. Ieda, S. Takahashi, S. Maekawa, and E. Saitoh, Nat. Phys. **12**, 52 (2016).

[50] R. Takahashi, H. Chudo, M. Matsuo, K. Harii, Y. Ohnuma, S. Maekawa, and E. Saitoh, Nat. Commun. **11**, 3009 (2020).

[51] R. J. Doornenbal, M. Polini, and R. A. Duine, J. Phys.: Mater. **2**, 015006 (2019).

[52] J. Fabian, A. Matos-Abiague, C. Ertler, P. Stano, and I. Žutić, Acta Phys. Slovaca **57**, 565 (2007).

[53] M. Drogeler, F. Volmer, M. Wolter, B. Terrés, K. Watanabe, T. Taniguchi, G. Guntherodt, C. Stampfer, and B. Beschoten, Nano Lett. **14**, 6050 (2014).

[54] M. H. Guimarães, A. Veligura, P. Zomer, T. Maassen, I. Vera-Marun, N. Tombros, and B. Van Wees, Nano Lett. **12**, 3512 (2012).

[55] E. C. Ahn, npj 2D Mater. Appl. **4**, 17 (2020).

[56] M. M. Glazov and E. L. Ivchenko, J. Exp. Theor. Phys. **99**, 1279 (2004).

[57] W. J. H. Leyland, G. H. John, R. T. Harley, M. M. Glazov, E. L. Ivchenko, D. A. Ritchie, I. Farrer, A. J. Shields, and M. Henini, Phys. Rev. B **75**, 165309 (2007).